3-D real-time motion correction in high-intensity focused ultrasound therapy.

Mathieu Pernot, Mickaël Tanter, Mathias Fink

3D Real-time Motion Correction in High Intensity Focused Ultrasound Therapy

Mathieu Pernot, Mickaël Tanter and Mathias Fink

Laboratoire Ondes et Acoustique

ESPCI, Université Paris VII, UMR CNRS 7587

10, rue Vauquelin, 75005 Paris, France

corresponding author : Mathieu Pernot

mathieu.pernot@loa.espci.fr

Running title: Motion tracking for HIFU therapy

3D Real-time Motion Correction in High Intensity Focused Ultrasound Therapy

Abstract. A method for tracking the 3D motion of tissues in real-time is combined with a 2D High Intensity Focused Ultrasound (HIFU) multi-channel system in order to correct for respiratory motion during HIFU therapy. Motion estimation is based on an accurate ultrasonic speckle tracking method. A pulse-echo sequence is performed for a subset of the transducers of the phased array. For each of these sub-apertures, the displacement is estimated by computing the 1D cross-correlation of the backscattered signals acquired at two different times. The 3D motion vector is then computed by a triangulation algorithm. This technique is experimentally validated in phantoms moving as fast as 40 mm s^{-1} , and combined with HIFU sequences. A real-time feedback correction of the HIFU beam is achieved by adjusting the delays of each channel. The sonications "locked on target" are interleaved with very short motion estimation sequences. Finally, *in-vitro* experiments of "locked on target" HIFU therapy are performed in fresh moving tissues.

Keywords: HIFU, focused ultrasound, therapy, motion tracking.

INTRODUCTION

High Intensity Focused Ultrasound (HIFU) is a promising technique for the treatment of tumours in a broad variety of organs, such as the liver (Ter Haar *et al.* 1989, Wang *et al.* 2002), the prostate (Chapelon *et al.* 1992, Foster *et al.* 1993, Chapelon *et al.* 1999), the kidney (Chapelon *et al*. 1992, Hynynen *et al.* 1995, Damianou 2003), the brain (Fry *et al.* 1954, Vykhodtseva *et al.* 1994) and the breast (Wu *et al.* 2003). In HIFU treatments, an ultrasonic probe generates a very small single lesion (usually about 1-3 mm lateral dimension). The treatment of a large tumour requires to scan mechanically or electronically the focus over the whole region of interest, interleaving the sonications with cooling periods to avoid near-field heating (Damianou and Hynynen 1993). However, accurate targeting of human abdominal tumours is difficult to maintain treatment can last several hours (Fan and Hynynen 1996). The displacement of abdominal organs due to breathing can be very large in comparison with the size of the focal zone. Several studies have shown that the pancreas, the liver and other abdominal organs can move as much as 20 mm over the breathing cycle with motion speeds of up to 15 mm s^{-1} (Bryan et al. 1984, Ross et al. 1990, Davies et al. 1994). Thus, the reliability and efficiency of treatment can be greatly reduced by breathing (Wang *et al.* 1994), and some cases of mistargeting have been reported recently by Allen *et al.* (2002) in HIFU treatment of liver metastases.

Motion tracking techniques have been widely investigated in medical applications such as radiotherapy and 3D imaging (MRI and CT). Respiratory gating is a conventional technique for addressing the problem of breathing motion in radiation therapy (Kubo and Hill 1996). External sensors (spirometer, strain gauge or infrared laser sensors on the patient's skin) are monitored during the treatment, and the therapeutic beam is switched off whenever the target is outside a predefined window. Internal metallic markers have recently been used in respiration gated radiotherapy (Shirato *et al.* 2000) to determine more accurately the 3D position of the tumour. But most of the current commercial systems allow the operator to monitor only the amplitude of displacement and not its direction. Indeed, although such systems can prevent a critical motion, no feedback is introduced in the therapeutic or imaging system to compensate for the motion.

In this study, we present an alternative ultrasound-based method for tracking and correcting the 3D motion of tissues in real-time during HIFU therapy. This technique is based on the tracking of temporal shifts in the backscattered RF signals (i.e. speckle) resulting from the displacements of the tissues. Speckle tracking techniques were widely investigated in diagnosis ultrasound (Bonnefous and Pesque 1986, Hein *et al.* 1993) and were successfully applied to various 2D motion estimation problems (Capineri *et al*. 2002, Tanter *et al.* 2002). In optics, a similar method based on the tracking of laser speckle has been developed to estimate the motion of a surface (Houghton *et al.* 1997) and is now used in the "padless optical mouse", a common input device for PCs.

The main advantage of ultrasound-based methods is the high penetration rate of ultrasound in the human body and their real-time capabilities. Hence, the natural ultrasonic scatterers in biological tissue can be used as markers to track the motion of tissues located deep within organs. In other words, unlike other motion tracking techniques, the method that we propose works without any implanted markers. This method can be easily integrated in a HIFU multi-channel system. Finally, another very important innovation of this method consists in using the 3D position information as a feedback for the HIFU system: the transmit delays are modified instantaneously in order to electronically steer the high-power ultrasonic beam towards the corrected location.

In this paper, the ultrasonic speckle tracking technique is adapted to the 3D motion estimation of a single location. The basic principles are presented and the 3D motion tracking technique is integrated into an existing HIFU multi-channel system with real-time capabilities. Simulations are performed to investigate the feasibility of the motion tracking technique. High power experiments coupled with real-time 3D motion tracking and correction are performed in tissue-mimicking (TM) phantoms and fresh bovine liver. Finally, the limitations of this technique are discussed, and improvements are suggested.

MATERIALS AND METHODS

3D motion estimation principle

3D displacement estimation is achieved using successive 1D axial displacement estimation performed along at least three different directions. Of course, this concept can be applied to any particular array geometry. However, for the sake of simplicity, we will consider in this paper only the configuration used in our experiments: a phased array presenting a spherical section centred at the geometrical focus (see Fig. 1). A set of *N* sub-apertures of the array is used in pulse-echo mode. By applying different delays on the single elements, each sub-aperture is pre-focused at a chosen, common location in the moving tissue. The normalized vector $\vec{a}_i(a_{ix}, a_{iy}, a_{iz})$ indicates the direction of the beam axis of the i^{th} sub-aperture.

An ultrasonic wave is transmitted by one sub-aperture to the predetermined location. Then, the backscattered signals coming from the randomly distributed scatterers of the medium (i.e. the speckle) are received by the elements of the same sub-aperture. Using classical sum-and-delay processing (Jensen 2000), a focus is achieved in reception, and the resulting signal is recorded in memory. The axial displacement is estimated in the time-domain by implementing a classical speckle tracking technique on successive RF signals: a 1-D cross-correlation algorithm enables us to estimate the time-shift due to the tissue displacement. Thus, one time-shift is estimated for each sub-aperture of the array, corresponding to the component of the 3D displacement vector $\vec{d}(d_x, d_y, d_z)$ along the sub-aperture beam axis. For transducer *i*, the time shift t_i is given by (where *c* is the sound velocity):

$$t_i = 2\frac{a_{ix}dx + a_{iy}dy + a_{iz}dz}{c} \qquad (1)$$

Once the *N* time-shifts have been successively estimated, the set of *N* linear equations given by eqn (1) is inverted in order to solve for the three components *dx*, *dy* and *dz* of the displacement vector. Of course, this set of equations would be completely determined if the time-shifts were estimated for at least three separate transducers. Although the estimation process would be faster in terms of insonification time, three transducers may not be optimal in terms of estimation robustness, and having more sub-apertures would allow the estimation to be more stable. Indeed, if the displacement vector is

normal to the beam axis of a sub-aperture, it induces a fast decorrelation of the speckle and the axial displacement becomes difficult to estimate accurately.

In order to avoid such a situation, we work with more than three sub-apertures and solve the over-determined set of linear equations by the least-square method. The set of linear equations is written in matrix form (see eqn (2)). In this formulation, a matrix A of size Nx3 is filled with the coefficients (a_{ij}), the j^{th} spatial component of the vector $\vec{a}_i(a_{ix},a_{iy},a_{iz})$. The vector t contains the N time-shifts, and d is the unknown displacement vector:

$$\begin{pmatrix} \\ t \\ \\ \end{pmatrix} = \frac{2}{c}\begin{pmatrix} \\ A \\ \\ \end{pmatrix} \cdot \begin{pmatrix} d \end{pmatrix} \qquad (2)$$

The pseudo-inversion of the matrix A is computed using singular value decomposition ($A=U.W.V$ where U is a Nx3 orthogonal matrix, W a 3x3 diagonal matrix and V a 3x3 orthogonal matrix), and the least-squares solution vector d is given by:

$$\begin{pmatrix} d \end{pmatrix} = \frac{c}{2}\begin{pmatrix} V \end{pmatrix} \cdot \begin{pmatrix} diag\ (1/w_j) \end{pmatrix} \cdot \begin{pmatrix} U^T \end{pmatrix} \cdot \begin{pmatrix} \\ t \\ \\ \end{pmatrix} \qquad (3)$$

The displacement estimation process is summarized in Fig. 2. It should be noted that in practical applications, the singular value decomposition is computed once, so that the vector displacement is obtained with one matrix multiplication, a very simple and fast operation.

Simulations

To investigate the feasibility of this technique, simulations of the motion estimation process were performed. The goal of these simulations was to elucidate several considerations on the sub-aperture dimensions and the performance of the estimation. Indeed, the maximum measurable displacement of the scatterers between two successive echo acquisitions is highly related to the size of the sub-aperture's focal spot, in other words to the directivity of the sub-aperture. Moreover, as the 3D motion

estimation process is based on axial displacement estimations, the direction of the scatterers' displacement with respect to the sub-aperture's beam axis is an important issue.

In order to optimise the configuration of the sub-apertures, the accuracy of the displacement estimation was investigated as a function of the sub-aperture diameter (from 10 mm to 50 mm). The sub-apertures were modelled using the impulse diffraction code PASS[1] (Cassereau and Guyomar 1988). Each transducer worked at 900kHz central frequency with a bandwidth of 40%, and was pre-focused at a depth of 120 mm. Scatterers with non-uniform echogeneicity were distributed randomly in a 3D volume (50x50x50 mm^3) with an average density of 1 mm^{-3}. The impulse response of the scatterers was computed to simulate the backscattered signal received by the sub-aperture, taking into account the directivity pattern of each transducer. The scatterer distribution was then translated to other locations, and a collection of impulse responses was computed (see Fig. 3). The angle θ between the displacement vector and the ultrasonic beam axis *Oz* could be varied from 0° to 180° and the displacement amplitude d from 0.15 mm to 3 mm (respectively $\lambda/10$ and 2λ, where λ is the wavelength).

Axial displacements between the initial position and translated positions were computed using a cross-correlation algorithm. The correlation coefficient was also computed, providing a good index of confidence of the cross-correlation performance. Finally, the simulation of the displacement estimation process was carried out in a moving tissue. Four sub-apertures of the large ultrasonic sparse array used in our experiments were modelled using the impulse diffraction simulation (see Fig. 4). Each subaperture was composed of 7 single-elements (8 mm in diameter, 900 kHz central frequency). The mean distance between the centres of two neighbouring sub-apertures was 94 mm. The random distribution of scatterers was moved along a complex 3D trajectory with a time increment of 0.1s, and at each increment the axial displacement was estimated on the four sub-apertures. Eqn (3) was then solved to estimate the 3D displacement.

[1] http://www.loa.espci.fr/pass/

Motion tracking/HIFU transducers set-up

Motion tracking experiments were performed using a 200-element ultrasonic sparse array. This high power ultrasonic probe was initially designed and optimised for HIFU transcranial therapy (Pernot *et al*. 2003). However, as described previously, the motion tracking technique can be used with most of the 2D ultrasonic multi-element arrays.

The 200 high-power piezocomposite transducers (8 mm in diameter, 0.5 cm^2 active area, 900 kHz central frequency, Imasonic, Besançon, France) were mounted in a sealed, spherically curved holder with a 120 mm radius of curvature. The focal zone dimensions of the HIFU probe were measured at low acoustic intensity (< 5 W cm^{-2}) in a tank filled with degassed water. A 0.4 mm PVDF (polyvinylidenefluoride) bilaminar calibrated hydrophone (Golden Lipstick model, SEA, Soquel, CA) was moved using a stepper-motor-controlled 3D positioning system (MM4006, Newport, Irvine CA). The -6 dB focal zone was (1.2×1.2×7.5) mm^3. The transducers were connected to a 200-channel electronic driving system. Each electronic channel was fully programmable and possessed its own emission/reception electronic board, which could deliver up to 16 electrical Watts. A more detailed description of this multi-channel system is given in previous works (Pernot *et al.* 2003). In water, the ultrasonic array could generate an acoustic intensity of 30 kW cm^{-2} at focus for 5s. Moreover, the transducer distribution was optimised for electronic beam steering in HIFU applications and the focus could be moved +/-15 mm radially and +/-20 mm axially from the geometric focus (Pernot *et al.* 2003).

Taking advantage of the great versatility of the multi-element technology, sub-apertures of variable size and shape could be designed for the array using clusters of small transducers. Four round shape sub-apertures of approximately 25-mm in diameter were designed for motion tracking applications (see Fig. 4). In this configuration, each sub-aperture is composed of 1 central element surrounded by 6 elements, and the diameter could be easily increased by adding more elements. In addition, in order to ensure the accuracy of the displacement estimation (Tanter *et al.* 2002), the angles between the beam axis of each sub-aperture were maximized.

Real-time motion tracking and correction

In emission mode, a pulse was focused at a predetermined location by one sub-aperture. This location was not exactly the heating focal spot of the array, but rather a few millimetres in front of the heating zone. This choice was made to avoid speckle modifications or thermal lens effects due to heating or necrosis, as will be explained in the discussion section. In this case of course, the motion estimated at this location was assumed to be the same as the motion of the heating focus. For the case of more complex spatial distributions of displacements vectors, a solution is proposed in the discussion section.

The backscattered signals coming back from the "motion control" spot were received by the transducers of the same sub-aperture and recorded by the electronics. The whole process was repeated for the three other sub-apertures focusing at the same location. The signals were collected on a computer, beamformed, stored in memory, and the axial displacements were estimated. The whole process lasted about 5ms, including the cross-correlations and the vector displacement estimation. Hence, 3D displacement could be estimated at frame rates as high as 200 Hz. Moreover, the low bandwidth of the connection between our electronics and the computer highly limited this frame rate. While it is not a critical issue at this time, vector displacement estimation could be implemented in hardware if one desired to increase the frame rate of motion estimation.

Once the displacement was estimated, a real-time correction was achieved on the therapeutic system. A phase shift was calculated for each of the 200 elements in order to electronically steer the HIFU beam to the new location. The phase shifts were transferred to the electronic system, and a sonication was performed at this new location. The successive sequences are shown in Fig. 5. The duty cycle, defined as the fraction of time the array is transmitting at high intensity, reached a value of 90% during the treatment. Small changes in the hardware to avoid communication between the PC computer and the HIFU system during the acquisition process would enable the duty cycle to reach levels much higher than 90%.

In-vitro experiments

In order to investigate the accuracy of the displacement estimates, motion tracking experiments were first performed in phantoms. A piece of PVA (Polyvinylalcohol) polymer of approximately 70x70x70 mm^3 was mounted on a stepper-motor-controlled 3D positioning system (MM4006, Newport, Irvine CA). The phantom could be translated at a maximum speed of 50 mm s^{-1} inside a tank filled with degassed water. A computer was used to program and control the 3D trajectories. Motion estimation sequences were performed at a frame rate of 20 Hz during the displacement.

Real-time motion tracking experiments coupled with HIFU sonications were also conducted in bovine liver. A piece of fresh degassed bovine liver was mounted on the stepper-motor-controlled 3D positioning system. In these experiments, the focus of the motion tracking sub-apertures was steered electronically 10 mm in front of the geometrical focus of the array. This was done to avoid speckle modifications caused by heating or necrosis at this location. The tissue sample was moved along simple 3D trajectories: linear displacements along the 3D axis directions or square displacements in planes defined by the axis directions. The motion estimation sequences were performed at a repetition rate of 10 Hz. Between two successive sequences, the displacement was calculated, the HIFU beam was steered electronically, and a sonication of 90 ms was performed at maximum power.

RESULTS

Simulations

The correlation coefficient of the axial displacement estimation is plotted in Fig. 6 for transducers of different dimensions, as a function of the angle between the ultrasonic beam axis and the displacement direction. The correlation coefficients reach a maximum when the displacement vector is parallel to the beam axis (i.e. $\theta=0°$ or $\theta=180°$) ; in this configuration the backscattered signals are time-shifted with very little signal decorrelation. On the other hand, when the displacement vector is perpendicular to the beam axis (i.e. $\theta=90°$), the backscattered signals are strongly decorrelated and the correlation coefficient reaches a minimum. Of course, the value of this minimum depends on the ratio between the displacement amplitude and the size of the focal zone. As shown in Fig. 6, for a given perpendicular

displacement, the smaller the transducer (i.e. the larger the focal zone), the better the correlation. Indeed, if the displacement is larger than the lateral focal spot, two successive backscattered echoes correspond to two uncorrelated random scatterers distributions and the correlation coefficient between the two successive backscattered echoes drops dramatically (see Fig. 6c).

Because the displacement vectors may be in any direction, the whole range of available angles must be considered. On the one hand, in order to maximize the correlation coefficient in every direction, transducers or sub-apertures must be chosen so that the focal zone is sufficiently large compared to the displacement. Moreover, by using relatively small sub-apertures, their relative distance can be increased and this improves the robustness of the triangulation process as seen in the research field of vector Doppler for flow imaging (Capineri *et al* 2002) or vector motion estimation for ultrasound based elastography (Tanter *et al* 2002). On the other hand, the focal zone should be reasonably small in order to confine the tracked region to a zone of a few wavelengths. As seen in Fig. 6a, the 20-mm diameter sub-aperture at 1 MHz can be considered a satisfactory compromise. Its focal zone lateral dimension corresponds to approximately 9 times the wavelength, and for displacements below 2 mm, the smallest correlation coefficient found in the displacement estimation was 0.9. As a consequence, tissue displacements in any direction at speed of 20 mm s^{-1} could be measured with a repetition rate of 10 Hz. Higher speeds could be estimated by simply increasing the repetition rate.

Finally, a complete sequence of 3D motion estimation was performed. The scatterers were moved along a 3D curve shown in Fig. 7, and the whole displacement lasted 10s. 3D displacement estimation was performed with a repetition rate of 10Hz, using the sub-apertures designed in Fig. 4. A very good agreement was found between the motion of the scatterers and the displacement estimates, as shown in Fig. 7. The distance between the final positions was found to be 1.15 mm, which is smaller than the HIFU focal zone dimension.

Phantom experiments

The accuracy of the displacement estimation was experimentally investigated in a piece of PVA phantom moving at a constant speed between 1 mm s^{-1} and 50 mm s^{-1}. The displacement was estimated at a frame rate of 20Hz and compared to the position recorded by the motion controller system. The average error on the estimated position is plotted in Fig. 8 as a function of the motion speed. The average correlation coefficient on the 4 sub-apertures is also plotted in Fig. 8. This coefficient provides a confidence index for the estimation performance. For speeds below 40 mm s^{-1}, the relative error increases slowly from 1% to 6%, and the correlation coefficient is quite good (>0.9). Above 40 mm.s^{-1}, the acquisition frame rate is not fast enough, the relative error increases rapidly, and the correlation coefficient falls below 0.9. However, simply increasing the acquisition frame rate can overcome this decorrelation effect.

HIFU experiments coupled with real-time motion correction

HIFU experiments coupled with tissue motion were performed in a bovine liver sample. Firstly, the sample was displaced along a straight line in the lateral direction at a speed of 10 mm s^{-1}. During the heating process, the sample was moved 10 mm to the left, then to the right, and finally to the left. During the complete displacement, which lasted 3 seconds, the tissue was sonicated with a focal intensity of 3000 W cm^{-2}. A necrosis of approximately 10 mm x 1.5 mm was achieved (see Fig. 9.a). Then, the same sonication was performed at another location of the liver sample, but this time, the displacement estimation and motion correction were performed with a frame rate of 10Hz in a zone located 10 mm in front of the focus. Fig. 9.b clearly shows the improvement of the necrosis localization. The lateral dimensions of the lesion are approximately 2 mm x 1.7 mm. It should be noted that although the sonication duration was the same in the two experiments, the necrosis was attained in a much shorter time at the targeted location in the motion corrected experiment since the heat deposit is locked on target.

In a second experiment, a piece of liver was moved along a two-dimensional curve. A 10-mm side square-ring lesion was achieved by moving the tissue in the focal plane at the speed of 8 mm s^{-1}. This "square-ring motion" of the liver sample was repeated three times for a total sonication duration of 15 seconds. Fig. 10.a shows the square ring necrosis. Then, a second sonication was performed with real-time motion tracking and correction. As Fig. 10.b shows, the lesion is well defined and localized since all the acoustic energy has been deposited at the target location. It should be noted that the necrosis size is quite important (~3 mm). This is not due to poor precision on displacement estimates, but rather to the fact that the heat deposit at the focus is much more important in the motion corrected experiment. Due to heat diffusion, it results in an enlarged necrosis area. This point is very important and illustrates another major advantage of the motion correction technique. As the acoustic energy is optimally deposited in space, the sonication time and power can be strongly decreased.

To address this point, the previous experiment was done again with a lower intensity at focus. Sonications with and without motion correction were performed with an intensity at focus of 800 W cm^{-2}. Fig. 11.a shows that in the uncorrected experiment, the square ring necrosis no longer appeared. Motion prevents the attainment of the necrosis threshold. In contrast, a very small necrosis of about 1.3 mm in diameter was achieved in the motion-corrected experiment as the whole heat deposit was applied at the same location (Fig. 11.b).

DISCUSSION

The goal of this work was to propose and demonstrate the feasibility of 3D real time motion tracking and feedback correction of the HIFU beam during ultrasonic treatments. The ability of transducer arrays driven by multi-channel electronic systems to provide a heating beam locked on target was demonstrated experimentally for *in vitro* moving tissue samples. Such motion correction is particularly important for the treatment of abdominal tumours where it is well known that respiratory motion induces important consequences. Firstly, correcting motion is the only way to ensure that the entirety of the targeted volume has been properly and totally treated. Secondly, it is also the only way to ensure

that no other unwanted location has been damaged. Thirdly, the "first proof" experiments presented in this paper allow us to open new discussions regarding the importance of motion correction in terms of HIFU treatment times. Indeed, it was clearly shown that the "locked on target" heating beam was much more efficient in terms of acoustic energy deposit at the targeted location than a non-corrected beam. The combination of organ motion and heat diffusion phenomena acts as an aberrating effect for the heat deposit. The motion correction technique can be seen as a way to correct such an aberration and optimise the heat deposit at the target. For a single focal spot target and a typical respiratory motion, we have shown that the HIFU treatment coupled with motion correction enables one to reach necrosis much more quickly than without this correction. Thus, treatment times and, consequently, the total acoustic intensity delivered to the body could be decreased by more than 3 times. In the case of a larger target volume, the motion correction technique can be coupled to any kind of existing "spot by spot" treatment procedure. Of course, the gain in terms of insonification time for larger volumes will have to be addressed carefully in future works.

A cause for potential concern is the effect of local changes in the speed of sound caused by the heating process. Indeed, because the motion tracking technique is based on detecting time-shifts, the displacement estimates depend on the sound speed in the medium and the dependence of sound speed on temperature must be addressed. First of all, in order to decrease the influence of the speed of sound variation with temperature, the displacements in our experiments were estimated in a zone located 10 mm in front of the focus (a non or slightly heated area). However, even in this configuration, the near field overheating may be a concern, especially for long treatments. To address this question, we considered the case of motion tracking in a tissue that undergoes a global temperature elevation. The variation of the speed of sound with temperature depends on the tissue type and the fat content (Miller *et al.* 2002), but is typically β=1m/s/°C in a liver of normal fat content. A temperature increase ΔT of the tissue would result in an apparent displacement of $\Delta l \sim 2\frac{L\,\beta\,\Delta T}{c}$, where L is the thickness of the penetrated tissue. For a 50 mm penetration depth the apparent displacement between two backscattered echoes would be 0.07 mm.°C^{-1} per 1°C temperature increase along the beam axis. This order of magnitude remains very small compared to the various motions caused by breathing.

Moreover, for a typical temperature increase of 30°C at the focus, an increase of 5°C is found 10 mm in front of the focus. Thus, estimating the 3D motion in this region should prevent the influence of this heating term.

The 3D motion tracking and correction process assumes that the displacement vectors of the heating target and the control focal spot are identical. In other words, it is assumed that no local rotations of the tissue are involved between these two points. However, even if we wanted to take into account this refinement for certain configurations, this point would not be a major issue. Indeed, in the case of such complex motion which mixes translations and rotations, the displacement field can be estimated at three different "motion control locations" instead of only one single location. In transmission mode, the number of emission pulses is multiplied by a factor three, but it does not really affect the HIFU beam duty cycle. The 3D motion tracking principle presented in the Method section can be applied to three different locations surrounding the heating focal spot. Fig. 12 illustrates such a process.

The estimation of motion vectors at three different locations surrounding the heating spot allows one to deduce the change of coordinate system (translation and rotation) of the medium from two successive acquisitions. First, the displacement vector $\vec{d}_i(d_{ix}, d_{iy}, d_{iz})$ is deduced from eqn (3) at each location *i*. The matrix $D = \{d_{ij}\}$ is then defined as the transfer matrix between two coordinate systems. Second, from the knowledge of *D*, and the spatial coordinates of the control points (F_1, F_2, F_3), the displacement of the heating spot can be easily computed and finally used for the feedback correction.

CONCLUSION

An ultrasound-based technique for real time 3D motion tracking and feedback correction in HIFU therapy was proposed and validated. This "first proof" study shows the ability of a multi-channel electronic platform driving HIFU multi-element arrays to provide a heating beam locked on a selected target. The 3D real-time motion tracking process was demonstrated experimentally for *in vitro* moving tissue samples. Phase shift corrections were applied in real-time on each element of the HIFU array in order to electronically steer the beam and correct the tissue displacements. Interleaving fast 3D motion tracking sequences with longer heating sequences at a typical repetition rate of 10-50 Hz allowed us to

ensure a “locked on target” HIFU beam. The motion correction technique wasted only a few percentage of the heating time, as the heating duty cycle reached more than 90 % in our experiments. Beyond the evident interest of motion correction for the improvement of HIFU targeting in abdominal organs, it was also shown that motion correction should lead to an important reduction of the treatment duration and total acoustic intensity deposit in the body.

REFERENCES

Allen M, Rivens I, Visioli A, Ter Haar G. Focused ultrasound surgery (FUS): a non-invasive technique for the thermal ablation of liver metastases, Proc. ISTU 2002, Seattle.

Bonnefous O, Pesque P. Time domain formulation of pulse-Doppler ultrasound and blood velocity estimation by cross correlation. Ultrason Imaging 1986 ;8;2:73-85.

Bryan PJ, Custar S, Haaga JR, Balsara V, Respiratory movement of the pancreas: an ultrasonic study." J Ultrasound Med. 1984;3:317-320.

Capineri L, Scabia M, Masotti L. A Doppler system for dynamic vector velocity maps. Ultrasound Med Biol 2002;28;2:237-48.

Cassereau D, Guyomar D. Computation of the impulse diffraction of any obstacle by impulse ray modelling – Prediction of the signals distortions. J. Acoust. Soc. Am. 1988; 84;4:1504–1516.

Chapelon JY, Margonari J, Theillere YA et al. Effects of high-energy focused ultrasound on kidney tissue in the rat and the dog. J Eur Urol 1992;22;2:147–152.

Chapelon JY, Margonari J, Vernier F. *et al.*, In vivo effects of high-intensity ultrasound on prostatic adenocarcinoma Dunning R3327. *Cancer Res* **52** 22, 1992, 6353–6357.

Chapelon JY, Ribault M, Vernier F, Souchon R, Gelet A. Treatment of localised prostate cancer with transrectal high intensity focused ultrasound. Eur J Ultrasound 1999 ;9;1:31–38.

Damianou C. In vitro and in vivo ablation of porcine renal tissues using high-intensity focused ultrasound. *Ultrasound Med. Biol.* 2003;29:1321-30.

Damianou C. and Hynynen K. Focal spacing and near-field heating during pulsed high temperature ultrasound therapy. *Ultrasound Med. Biol.* 1993 19:777-87.

Davies SC, Hill AL, Holmes RB, Halliwell M, Jackson PC. Ultrasound quantitation of respiratory organ motion in the upper abdomen. *Br J. Radiol*. 1994;67;1096-102.

Fan X, Hynynen K Ultrasound surgery using multiple sonications--treatment time considerations. Ultrasound Med Biol 1996;22:471-82.

Foster RS, Bihrle R, Sanghvi NT, Fry FJ and Donohue JP, High-intensity focused ultrasound in the treatment of prostatic disease. *Eur Urol* **23** Suppl. 1 (1993), pp. 29–33.

Fry W, Mosberg W, Barnard J, Fry F. Production of focal destructive lesions in the central nervous system with ultrasound. J Neurosurg 1954 ;11: 471–478.

Hein IA., O'Brien WD. Current time-domain methods for assessing tissue motion by analysis from reflected ultrasound echoes: A review. IEEE Trans. Ultrason. Ferroelect. Freq. Contr. 1993;40;2:84 –102.

Hossack J, Sumanaweera T, Napel S, Ha J. Quantitative 3-D diagnostic ultrasound Imaging using a modified transducer and an automated image tracking technique. IEEE Trans. Ultrason., Ferroelec., Freq. Contr. 2002;49;8:1029-1038.

Houghton A, Rees G and Ivey P. A method for processing laser speckle images to extract high-resolution motion. Meas. Sci. Technol. 1997; 8: 611-617.

Hynynen K, Damianou CA, Colucci V et al. MR monitoring of focused ultrasonic surgery of renal cortex: Experimental and simulation studies. J Magn Reson Imaging 1995;5;3: 259–266.

Jensen J.A. Ultrasound Imaging and its modelin*g*, "Imaging of Complex Media with Acoustic and Seismic Waves", Topics in Applied Physics, Springer Verlag, 2000.

Kubo H, Hill B. Respiration gated radiotherapy treatment : a technical study. Phys. Med. Biol. 1996, 41;1: 83-91.

Le Floch C, Tanter M and Fink M, Self defocusing in hyperthermia: experiments and simulations, *Appl. Phys. Lett.*, 74, 20, 1999, pp. 3062-3064.

Miller NR, Bamber JC, Meaney PM. Fundamental limitations of non-invasive temperature imaging by means of ultrasound echo strain estimation. Ultrasound Med Biol 2002; 28; 10: 1319-1333.

Pernot M, Aubry JF, Tanter M, Thomas JL, Fink M. High power transcranial beam steering for ultrasonic brain therapy. Phys. Med. Biol. 2003*;* 48 ;16: 2577-2589.

Ross CS, Hussey DH, Pennington EC et al. Analysis of movement of intrathoracic neoplasms using ultrafast computed tomography. *Int J Radiat Oncol Biol Phys.* 1990;18;671-677.

Shirato H, Shimizu S, Kunieda T *et al*. Physical aspects of a real-time tumor-tracking system for gated radiotherapy. Int. J. Radiation Oncology Biol. Phys., 2000; 48; 4: 1187-1195.

Simon C, VanBaren P and Ebbini E, Two-dimensional temperature estimation using diagnostic ultrasound, *IEEE Trans. Ultrason., Ferroelect., Freq., Contr.*, 1998, 45 pp. 1088-1099.

Schweikard A, Glosser, G, Bodduluri M, Murphy M, Adler J, Robotic motion compensation for respiratory movement during radiosurgery. *Computer Aided Surgery.* **4**;pp. 263-277, 2000.

Tanter M, Bercoff J, Sandrin L, Fink M. Ultrafast compound imaging for 2-D motion vector estimation: apllication to transient elastography. IEEE Trans. Ultrason., Ferroelec., Freq. Contr. 2002;49;10: 1363-1374.

Ter Haar G, Sinnett D, Rivens I. High intensity focused ultrasound—A surgical technique for the teatment of discrete liver tumors. Phys Med Biol 1989;34;11:1743–1750.

Vykhodtseva NI, Hynynen K, Damianou C. Pulse duration and peak intensity during focused ultrasound surgery: Theoretical and experimental effects in rabbit brain in vivo. Ultrasound Med Biol 1994;20;9: 987–1000.

Wang H, Ebbini ES, O'Donnell M, Cain CA. Phase aberration correction and motion compensation for ultrasonic hyperthermia phased arrays: experimental results. IEEE Trans. Ultrason., Ferroelec., Freq. Contr. 1994;41;1:34-43.

Wang Z, Bai J, Li F *et al.* Study of a "biological focal region" of High-intensity focused ultrasound. Ultrasound Med Biol 2003;29;5: 749-754.

Wu F, Wang Z, Cao Y *et al.*, Changes in biologic characteristics of breast cancer treated with high-intensity focused ultrasound**,** *Ultrasound Med Biol.*, 29, 10, 2003, 1487-1492.

FIGURE CAPTIONS

Fig. 1: 3D Motion tracking set-up using three transducers or sub-apertures distributed on a spherical section. (*dx*,*dy*,*dz*) is the displacement vector of the scatterers.

Fig. 2: 3D vector displacement estimation process using N transducers or sub-apertures. At time *t*, *N* backscattered signals are recorded and stored in memory. At time $t+\Delta t$, *N* new signals are recorded and cross-correlated with the previous ones. *N* time-shifts are determined and used in a trangulation algorithm to compute the displacement vector.

Fig. 3: Sub-aperture configuration. The backscattered signal is analysed as a function of the sub-aperture diameter *L* and the scatterers distribution displacement vector (d,θ).

Fig. 4: Four sub-apertures designed on the quasi-random phased array used in motion tracking experiments.

Fig. 5: HIFU sonications interleaved with motion tracking sequences. After each motion tracking sequences delays are applied to the electronic channels, in order to electronically steer the HIFU beam.

Fig. 6: Correlation coefficients as a function of the displacement directions and displacement amplitude (– 0.1 ; — 0.5 ; – 1 ; –. 1.5 ; .. 2 ; – 2.5 mm). Different size of transducers are investigated a) 20 mm, b) 30 mm and c) 50 mm.

Fig. 7: Tracking of a complete 3D motion: – scatterers motion, –● displacement estimates.

Fig. 8: Displacement estimation accuracy as a function of the motion speed. The – curve is the relative error on the displacement estimates, and the -- curve is the correlation coefficient.

Fig. 9: Necrosis induced in liver moving at 10 mm/s a) without motion correction b) with motion correction.

Fig. 10: Square shaped necrosis induced in liver moving at 8 mm/s in the focal plane a) without motion correction b) with motion correction. The intensity at focus was 3000 W cm^{-2}.

Fig. 11: Square shaped necrosis induced in liver moving at 8 mm/s in the focal plane a) without motion correction b) with motion correction. The intensity at focus was 800 W cm^{-2}.

Fig. 12: Three "motion control locations" set-up in the case of complex motion (Translation + Rotation). The 3D motion estimation process achieved using at least three sub-apertures, is applied to three different locations F_1, F_2 and F_3.

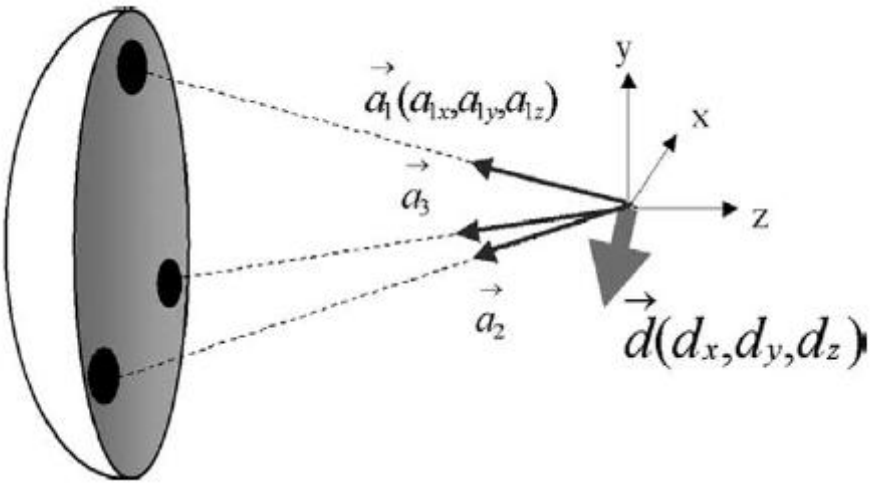

Figure 1.

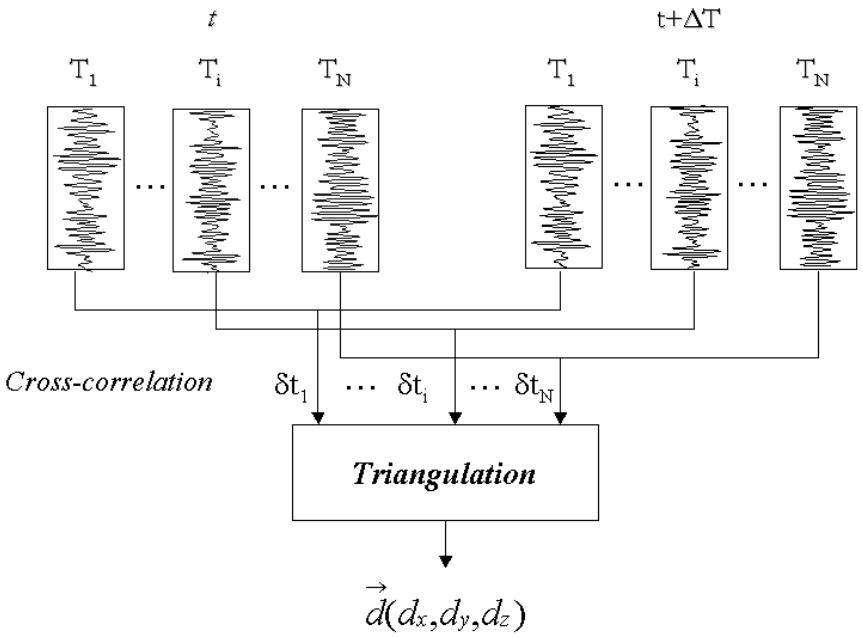

Figure 2

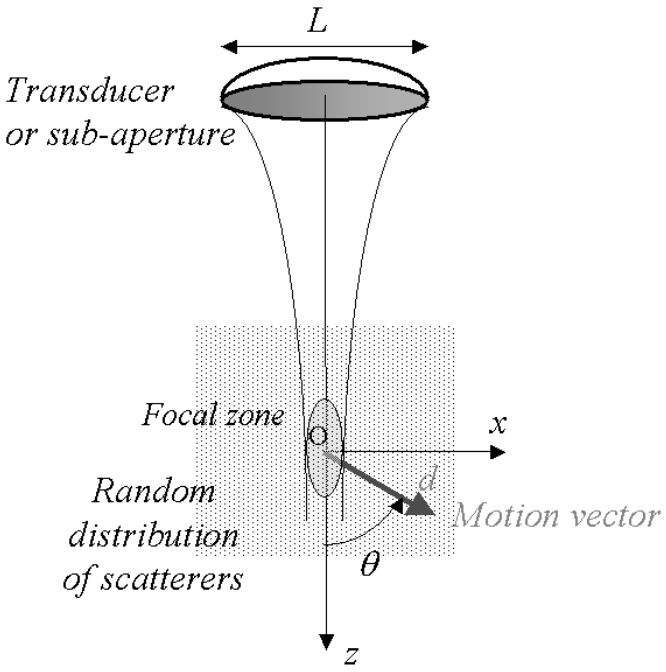

Figure 3

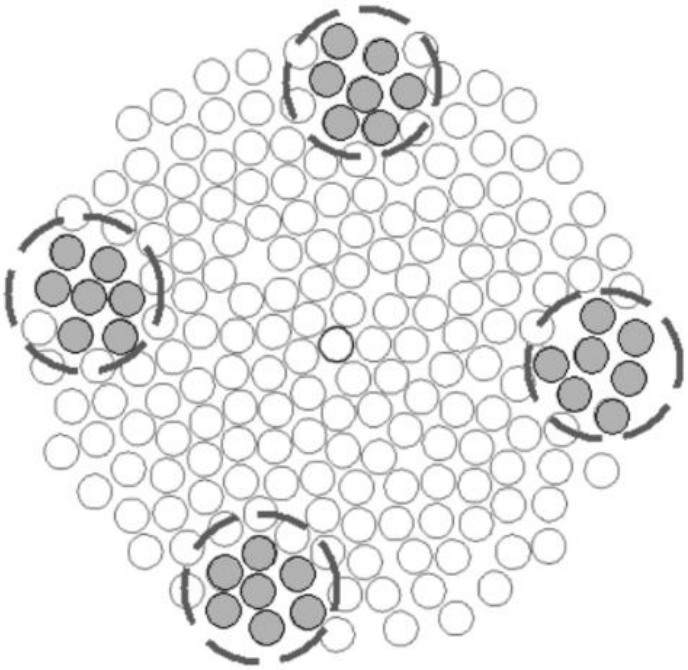

Figure 4

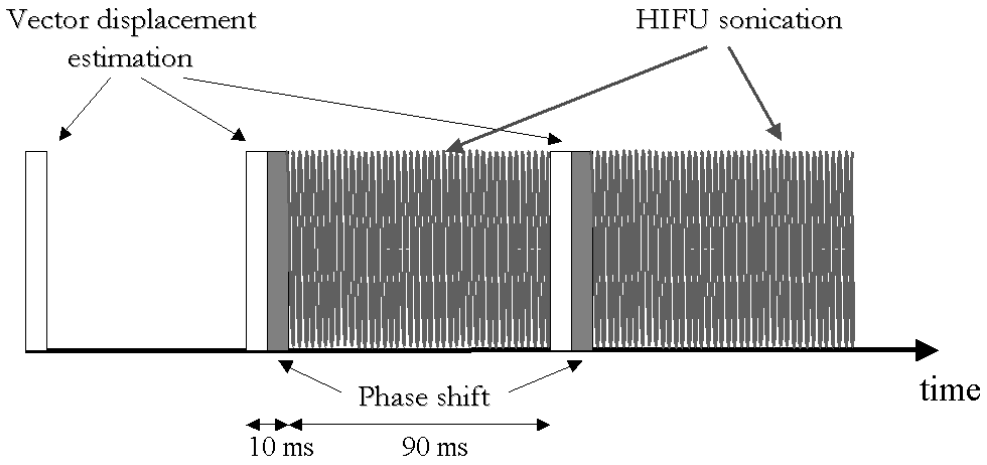

Figure 5

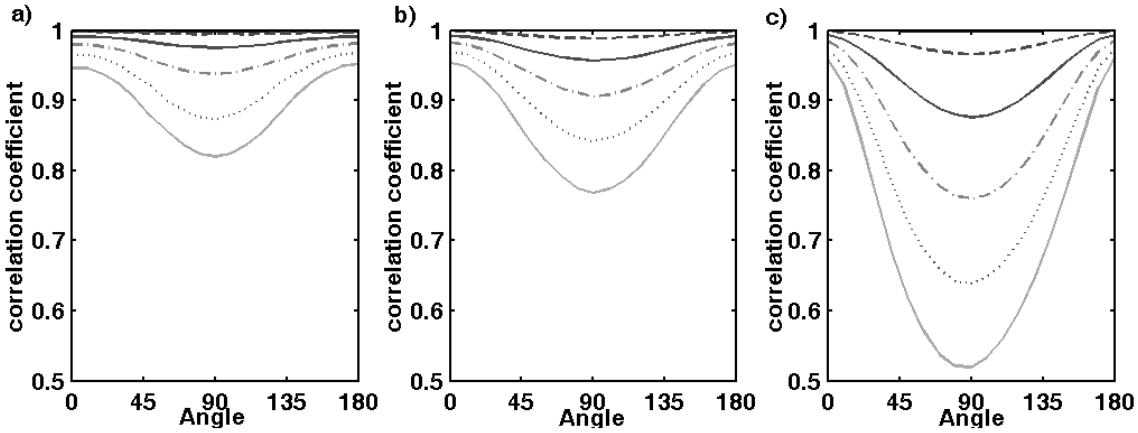

Figure 6

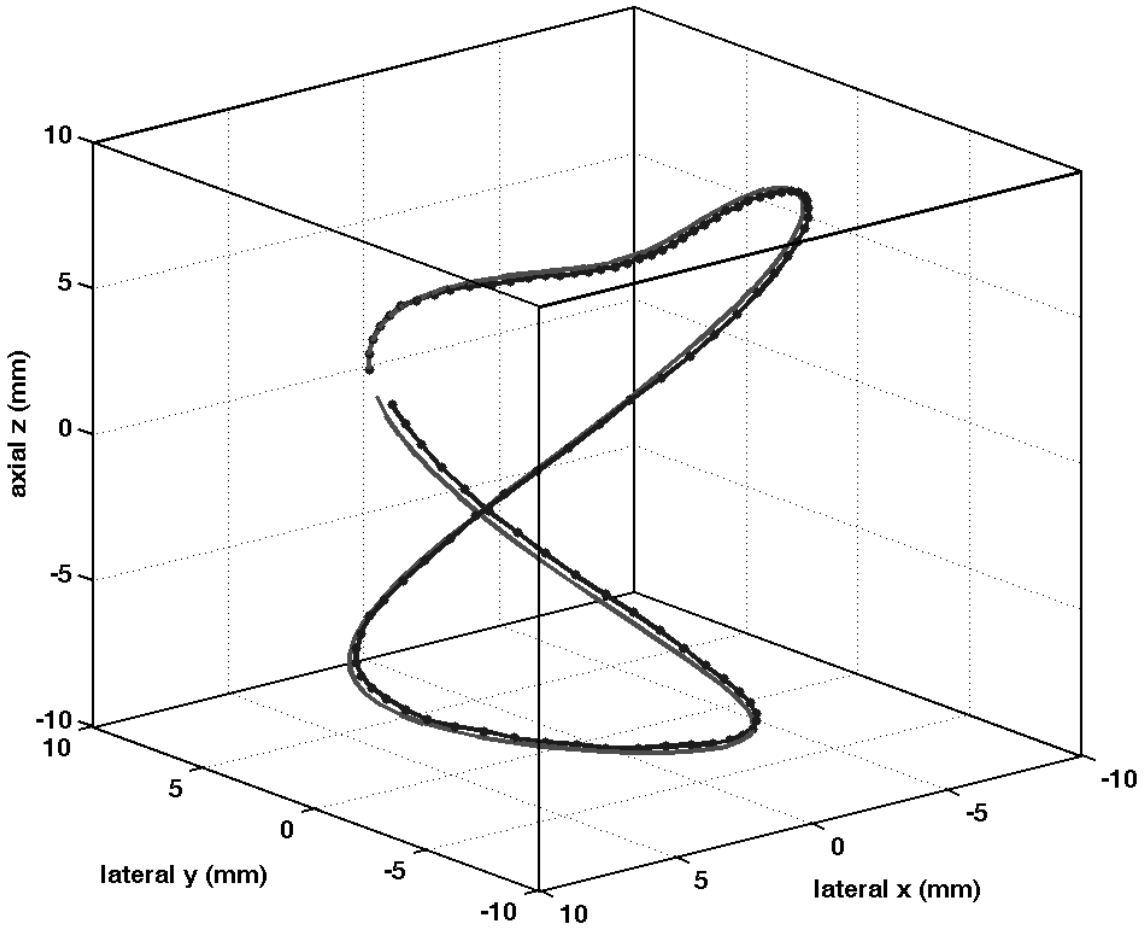

Figure 7

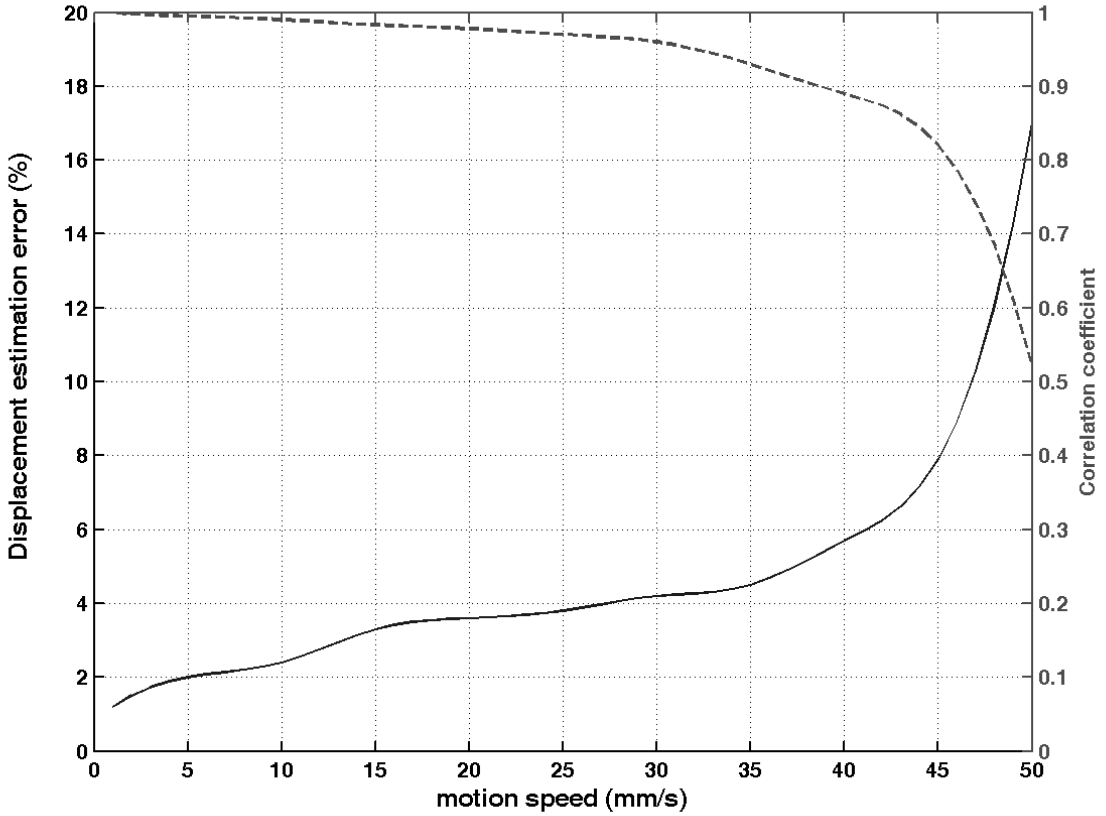

Figure 8

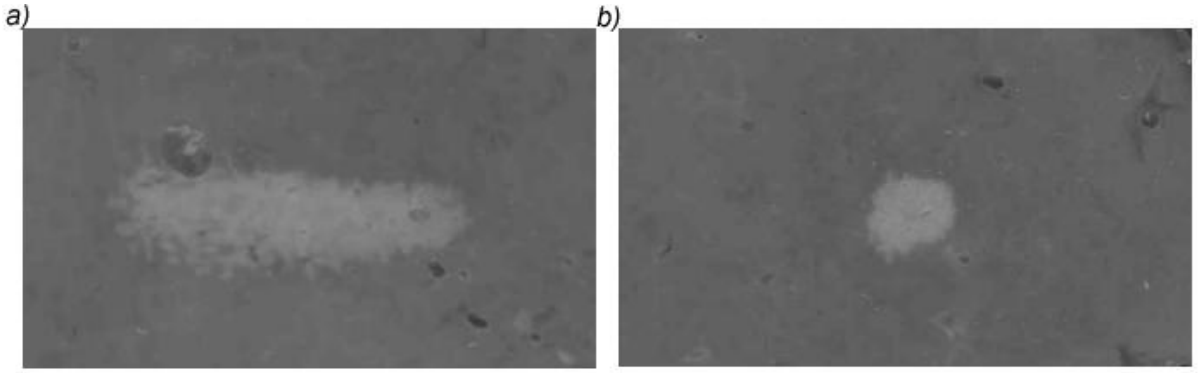

Figure 9

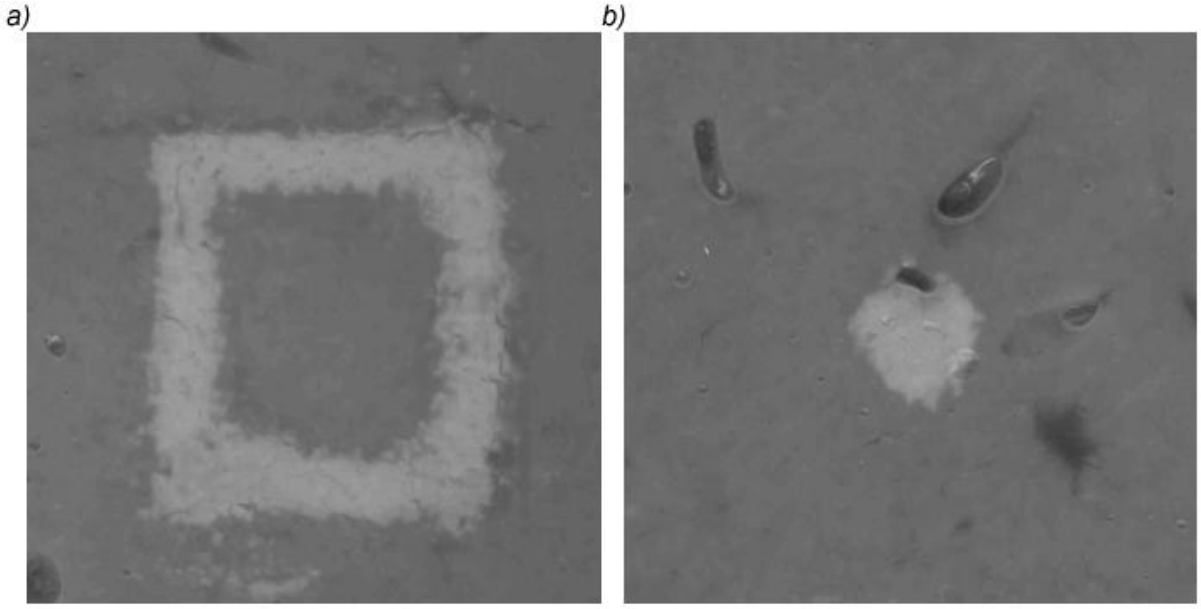

Figure 10

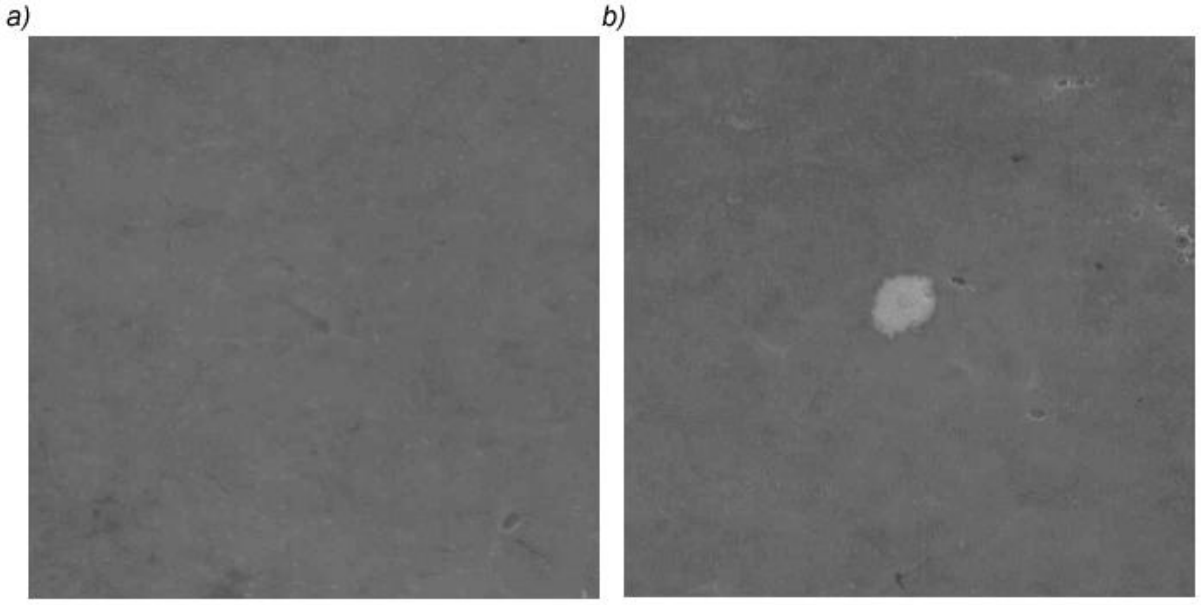

Figure 11

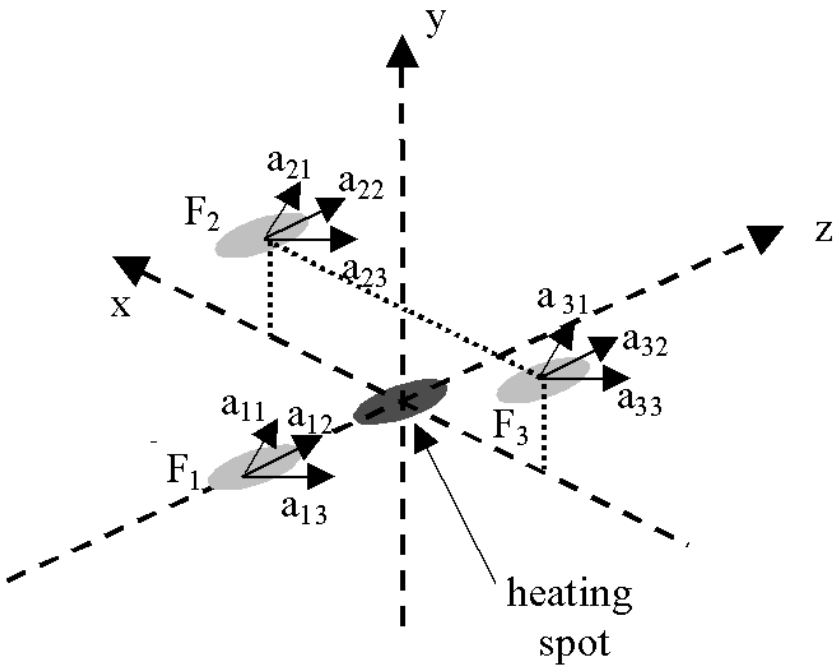

Figure 12